Computational Materials Science 50 (2011) 811–819

Contents lists available at ScienceDirect

Computational Materials Science

journal homepage: www.elsevier.com/locate/commatsci

Kinetic modeling of high temperature oxidation of Ni-base alloys

A. Chatterjee [a,*], S. Srikanth [a], S. Sanyal [a], L. Krishna [a], K. Anand [a], P.R. Subramanian [b]

[a] GE Global Research Center, Bangalore, India
[b] GE Global Research Center, Niskayuna, NY, USA

ARTICLE INFO

Article history:
Received 5 May 2010
Received in revised form 28 September 2010
Accepted 4 October 2010
Available online 9 November 2010

Keywords:
Ni-based superalloy
Thermodynamic model
Oxidation kinetics
Genetic algorithm based optimization
Wagner's equation

ABSTRACT

The rates of isothermal and cyclic oxidation and the elemental concentration profiles as a function of time of oxidation for a few Ni-base superalloys were determined through a modified Wagner's oxidation model and the solution of coupled elemental diffusion equations. Thermodynamically calculated interfacial elemental concentrations and oxygen partial pressures for the multi-component Ni-base alloys were used as boundary conditions for the solution of Wagner's equation and the elemental coupled diffusion equations (for Cr, Al and O). The multiple elemental diffusion and mass conservation equations were solved using a numerical procedure. The dependence of self/tracer-diffusivities of Cr, Al and O in the corundum phase on the oxygen partial pressures was deduced using a genetic algorithm based optimization procedure incorporating the experimental parabolic rate constants for several Ni-base alloys. Rates of cyclic oxidation were then deduced from the deterministic interfacial cyclic oxidation spalling model (DICOSM) developed by Smialek [1]. The calculated oxidation rates were in reasonable agreement with the experimental values for a range of multi-component Ni-base alloys.

1. Introduction

Further improvement in the development of Ni-base superalloys for higher temperature applications in gas turbines and aero-engines to improve the energy efficiency is constrained by their high temperature corrosion. Knowledge of the rates of oxidation of these alloys as a function of temperature and gas composition is essential for this purpose. Since high temperature isothermal or cyclic corrosion experiments under simulated gas atmospheres are both time consuming and expensive, modeling the rates of isothermal and cyclic oxidation of multi-component multiphase alloys is essential for the design of Ni-base superalloys and bond coat alloys. The oxidation rate of alloys is determined both by thermodynamic and kinetic considerations. A rigorous thermodynamic analysis of the oxidation of multi-component multiphase Ni-base alloys was reported in an earlier study [2]. In this paper, we would restrict to the analysis of the kinetics of oxidation of these alloys.

The early theories on the kinetics of oxidation were based on the Tammann–Pilling–Bedworth (TPB) parabolic law derived from Fick's law of diffusion under various assumptions. The basic assumptions of the TPB parabolic law are the following:

- The growth of the oxide phase is by atomic/molecular diffusion.
- The diffusion coefficient is independent of the concentration.
- The elemental concentrations at the alloy/oxide and oxide/gas interfaces are independent of the scale thickness.
- Oxidation occurs at steady state.

The rate of oxide layer growth is given as:

$$\frac{dL(t)}{dt} = \frac{V_{\text{oxide}} D[C(0) - C(L)]}{L(t)} \tag{1}$$

Integration of the above equation, yields the parabolic law i.e.,

$$L(t)^2 = 2kt$$
$$k = V_{\text{oxide}} D[C(0) - C(L)]$$

where V_{oxide} is the molar volume of the oxide, $L(t)$ is the thickness of the oxide scale at time t, $C(0)$ and $C(L)$ are the concentration of the diffusing species at the alloy/oxide and oxide/air interfaces respectively, k is the rate constant and D is the intrinsic diffusivity of the diffusing species. Subsequently, Wagner [3] postulated that the oxidation of metals occurs by the transport of charged defects in oxides and developed a theory based on the theoretical treatment of ionic diffusion in electrolytes. Wagner's equation is essentially based on the linear diffusion equation for charged particles:

$$J_i = \frac{D_i C_i}{kT}\left[-\frac{d\mu_i}{dx} + q_i E\right] \tag{2}$$

where J_i is the flux of the ith species, μ_i is the chemical potential, C_i is the concentration (number of particles per unit volume) of the diffusing charged defect, q_i is the effective charge on the defect, E

* Corresponding author. Tel.: +91 80 4088 3927; fax: +91 80 2841 2111.
E-mail address: aveek.chatterjee@ge.com (A. Chatterjee).

0927-0256/$ - see front matter © 2010 Elsevier B.V. All rights reserved.
doi:10.1016/j.commatsci.2010.10.006

the electric field, k is the Boltzmann constant, and T is the temperature. For each diffusing species, flux equations similar to Eq. (2) can be given. Eq. (2) is based on the validity of the Nernst–Einstein relationship and is therefore applicable only for thick oxide scales (>1 μm) and at temperatures greater than 500 °C. By assuming the magnitude of the electric field to be small and assuming charge neutrality and local equilibrium at all points within the oxide phase, we can eliminate from the coupled transport equations, the electric field and all the chemical potentials, except that of oxygen and correlate the parabolic rate constant (k_p) to the tracer diffusion coefficients of the cations [$D^*(M)$] and anions [$D^*(O)$]:

$$k_p = \int_{p_{O_2(I)}}^{p_{O_2(II)}} \left[\frac{\alpha D^*(M)}{f_M} + \frac{D^*(O)}{f_O}\right] d\ln p_{O_2} \tag{3}$$

where $\alpha = a/b$ is the stoichiometric ratio of the oxide phase (M_aO_b), f_M and f_O are the correlation factors for the metal and oxygen ions for self diffusion and is of the order of unity, $p(O_2)_I$ and $p(O_2)_{II}$ are the oxygen partial pressures at the metal/oxide and oxide/gas interfaces respectively. To evaluate the parabolic rate constants using Eq. (3), a knowledge of the cation and anion tracer diffusion coefficients as a function of the oxygen partial pressure is essential. The functional relationship between tracer diffusion coefficients and oxygen partial pressure depends on the defect chemistry of the oxide [4]. Tretjakow and Schmalzreid [4], Gesmundo and coworkers [5] and Dieckmann [6] give a detailed treatise on the effect of defect chemistry of various oxides on metal oxidation. If the oxide formation is controlled purely by oxygen ion diffusion, the $D^*(M)$ term can be neglected and if it is controlled by cation interstitials diffusion, the $D^*(O)$ term can be neglected. The main difficulties with the application of Wagner's theory are:

1. Knowledge of defect chemistry and transport mechanism in the oxide scale is essential.
2. Defect chemistry and the diffusivities of the mobile species are a function of oxygen partial pressure and therefore p_{O_2} dependence of D^* in the oxide may be different at metal/oxide and oxide/air interface.
3. Gets complicated when more than one oxide phase forms – e.g., corundum, spinel, rocksalt/monoxide, etc.
4. Diffusivity along grain boundaries and dislocations may have different p_{O_2} dependence and coupling them in Wagner's equation may be difficult.

Application of Wagner's theory to complex oxide growth is rendered difficult because of the uncertainties concerning the defect and transport properties of multi-component oxide solutions.

Some papers on the modeling of oxidation of ternary Ni-base alloys have been reported in the literature. Nijdam et al. [7,8] reported a coupled thermodynamic–kinetic oxidation model to describe the thermal oxidation of a γ-phase Ni–27Cr–9Al (at.%) alloy at 1373 K. They have used the THERMOCALC™ software [9] and the TTNI7 [9] database for the determination of the activities of the constituents in the alloy phase. For a given oxide layer growth kinetics (i.e., using experimental growth rates), the model computes composition–depth profiles in the alloy as well as the amount of each oxide phase developed as a function of oxidation time. In their kinetic approach, elemental diffusion equations have been formulated for the alloy phase. Whereas, diffusion of mobile charged species within the oxide phase is not implicitly considered (experimental parabolic rate constants in the oxide phase is directly used). The chemical diffusion coefficients as a function of composition in the alloy phase have also been taken from the mobility database of DICTRA™ [9]. We are not aware of any paper in the literature where the activities in the oxide phase are also considered in the modeling of oxidation. Further there is no literature on the modeling of oxidation of multi-component Ni-base alloys.

In the present work, mathematical models based on genetic algorithm (GA) were developed to extract the diffusivities of multi-component alloys. The diffusivities were then used in a cyclic oxidation model for analysis of high temperature oxidation of Ni-base alloys. The predicted oxidation rates were compared with experimental data.

2. Mathematical models and computational methods

2.1. 2A. Modeling of oxidation of multi-component alloys

In the present study on the modeling of the kinetics of oxidation of multi-component alloys, two approaches were considered: (i) a modified Wagner's ionic approach and (ii) simultaneous solution of multiple elemental diffusion equations. In an earlier paper on the thermodynamics of oxidation of multi-component Ni-base alloys, it was observed that three different oxide phases formed, i.e., corundum (solid solution of Al_2O_3 and Cr_2O_3) formed adjacent to the alloy at low p_{O_2} followed by the alloy-corundum-spinel (solution of $NiCr_2O_4$–$NiAl_2O_4$) equilibria as p_{O_2} is increased and then the spinel–bunsenite (NiO) equilibrium up to the oxide/air interface. Also, there is ample literature evidence [8,43] that highlight the co-existence of multiple oxides, viz. Cr_2O_3 and NiO above Al_2O_3 scale. This is also reinstated by the XRD analyses reported in literature [30]. However, consideration of all the elements and all the oxide phases makes the kinetic treatment mathematically unwieldy. Further, diffusivity data of all the elements in the different oxide phases and their temperature and oxygen partial pressure dependence are not available in the literature. Keeping this in mind, our approach has been to extract D from K_p, which was experimentally available. We also established a method using genetic algorithm to extract a unique value of diffusivity from several sets of experimental K_p. Besides, the dependence of K_p on p_{O_2} has been incorporated in the optimization model. Further details of the optimization method used has been presented in Section 2.5. For simplicity, we have made the following assumptions:

1. Diffusion in the oxide product phase is the rate-controlling step.
2. The diffusivity of Al in alloy, as quoted from DICTRA [44], is of the order of 10^{-13}–10^{-14} cm^2/s at 1100 °C, whereas, diffusivity of Al and O in the oxide (Al_2O_3) is of the order of 10^{-17} cm^2/s. Since the elemental diffusivities in the alloy phase are two to three orders of magnitude greater than their corresponding diffusivities in the oxide phase, the existence of a concentration profile within the alloy is neglected.
3. The formation of only the corundum oxide phase is considered. The subsequent formation of the spinel and bunsenite (NiO) phases is ignored for oxide growth. However, the co-existence of the corundum phase with the spinel phase is considered for the determination of elemental concentration profiles in the corundum oxide phase.
4. Diffusion of only the major species i.e. Cr, Al and O in the oxide phase is considered. The diffusion model does not specify the nature of the diffusion process (e.g. grain boundary diffusion, bulk diffusion, etc.).
5. The solubility of oxygen in the alloy is considered to be negligible.

2.2. Modified Wagner's equation for multi-component alloys

Wagner's approach can be adopted for a multi-component oxide and an equation can be derived (assuming charge neutrality

and local equilibrium at all points within the oxide phase) for the parabolic rate constant in terms of the diffusivities of all the charged defects (oxygen ion, all the cation interstitials and electrons). The modified Wagner equation correlating the parabolic rate constant to the ionic diffusivities for a multi-component (comprising of N cations) oxide phase can be given as:

$$k_p = \int_{p'_{O_2}}^{p''_{O_2}} \left[\sum_{i=1}^{N} \alpha \frac{D^*_{i,\mathrm{eff}}(M_i)}{f_{m_i}} + \frac{D^*_{\mathrm{O,eff}}(\mathrm{O})}{f_{\mathrm{O}}} \right] d\ln p_{O_2} \tag{4}$$

where $\alpha = b/a$ is the stoichiometric factor for oxide M_aO_b, f_{mi} and f_O are the correlation factors for the individual cations and oxygen ion self-diffusion mechanisms and are of the order of unity. $D^*(M_i)$ and $D^*(O)$ are the effective cation and oxygen ion self-diffusion coefficients and are a function of both oxygen partial pressure and temperature. The effective diffusion coefficients accounts for diffusion through the lattice, grain boundaries and defects and is given by:

$$D^*_{i,\mathrm{eff}} = D^*_{\mathrm{eff}} p_{O_2}^{1/n_i}$$

$$D^*_{\mathrm{eff}} = (1-f)D_L + f.D_{gb}$$

$$f = \frac{2\delta}{\mu} \tag{5}$$

where n_i is the functional dependence on p_{O_2} depending on defect structure and can be positive or negative depending on the defect, f is the effective volume fraction of grain boundaries; δ is the grain boundary width and μ is the grain size. In this study, we have considered only the effect of p_{O_2} on diffusivity and assumed that the concentration of other elements in the oxide phase alters the diffusivity by altering the p_{O_2}.

2.3. Formulation of diffusion equations in the alloy and oxide phases

Similar to the Tammann–Pilling–Bedworth approach, diffusion and mass conservation equations can be formulated for all the elements and for each of these phases, assuming mass transport in the alloy and oxide phases to occur through atomic transport. However, as mentioned earlier, consideration of all the elements and all the oxide phases makes the kinetic treatment mathematically unwieldy and therefore, the same assumptions as mentioned earlier were made for formulating the diffusion equations.

Based on Fick's 2nd law, the concentration profiles for Cr, Al and O in the corundum phase as a function of time can be given as:

$$\frac{\partial C^{\mathrm{cor}}_{\mathrm{Cr}}}{\partial t} = \frac{\partial}{\partial X} D^{\mathrm{cor}}_{\mathrm{Cr}} \frac{\partial C^{\mathrm{cor}}_{\mathrm{Cr}}}{\partial X} \tag{6}$$

$$\frac{\partial C^{\mathrm{cor}}_{\mathrm{Al}}}{\partial t} = \frac{\partial}{\partial X} D^{\mathrm{cor}}_{\mathrm{Al}} \frac{\partial C^{\mathrm{cor}}_{\mathrm{Al}}}{\partial X} \tag{7}$$

$$\frac{\partial C^{\mathrm{cor}}_{\mathrm{O}}}{\partial t} = \frac{\partial}{\partial X} D^{\mathrm{cor}}_{\mathrm{O}} \frac{\partial C^{\mathrm{cor}}_{\mathrm{O}}}{\partial X} \tag{8}$$

In Eqs. (6)–(8), $D^{\mathrm{cor}}_{\mathrm{Cr}}$, $D^{\mathrm{cor}}_{\mathrm{Al}}$, and $D^{\mathrm{cor}}_{\mathrm{O}}$ are intrinsic diffusion coefficients of Cr, Al, and O respectively in the corundum phase and are functions of the oxide composition and temperature. Eqs. (6)–(8) can also be written in terms of the elemental chemical potential gradients and self-diffusion coefficients rather than concentration gradients and chemical diffusion coefficients. The concentration mentioned in Eqs. (6)–(8) refer to the active and mobile species, which participate in the oxidation process. Thermodynamic modeling can be used to generate either the interfacial chemical potentials or concentrations for a multi-component multiphase system for the solution of the diffusion equations. The elemental mass conservation equations at the alloy/corundum interface are:

$$v_{\mathrm{alloy/cor}}\left(C^{\mathrm{alloy/cor,int}}_{\mathrm{Cr}} - C^{\mathrm{cor}}_{\mathrm{Cr}}\right) = D^{\mathrm{cor}}_{\mathrm{Cr}} \frac{\partial C^{\mathrm{cor}}_{\mathrm{Cr}}}{\partial X} \tag{9}$$

$$v_{\mathrm{alloy/cor}}\left(C^{\mathrm{alloy/cor,int}}_{\mathrm{Al}} - C^{\mathrm{cor}}_{\mathrm{Al}}\right) = D^{\mathrm{cor}}_{\mathrm{Al}} \frac{\partial C^{\mathrm{cor}}_{\mathrm{Al}}}{\partial X} \tag{10}$$

$$v_{\mathrm{alloy/cor}}\left(C^{\mathrm{alloy/cor,int}}_{\mathrm{O}} - C^{\mathrm{cor}}_{\mathrm{O}}\right) = -D^{\mathrm{cor}}_{\mathrm{O}} \frac{\partial C^{\mathrm{cor}}_{\mathrm{O}}}{\partial X} \tag{11}$$

where $v_{\mathrm{alloy/cor}} = dX_{\mathrm{alloy/cor}}/dt$ is the velocity of the alloy/corundum interface i.e., rate of growth of the corundum phase. It is appropriate to mention that since the interface position is determined by the fastest diffusing species, mass conservation equation will apply only for this species. Therefore, among Eqs. (9)–(11) for the alloy/corundum interface, only one of them is relevant and the remaining equations are redundant. The initial conditions at $t = 0$ is given as:

$$\begin{aligned} &C^{\mathrm{alloy/cor,int}}_{\mathrm{Cr}} = C^{0}_{\mathrm{Cr}}; \quad C^{\mathrm{alloy/cor,int}}_{\mathrm{Al}} = C^{0}_{\mathrm{Al}}; \\ &C^{\mathrm{cor}}_{\mathrm{Cr}} = 0; \quad C^{\mathrm{cor}}_{\mathrm{Al}} = 0; \end{aligned} \tag{12}$$

At all times t, the alloy/corundum (1st interface) and the corundum/spinel interfaces (2nd interface) are at thermodynamic equilibrium and therefore, the boundary conditions at the interfaces at any given time t are given by:

$$\begin{aligned} &C^{\mathrm{alloy,int1}}_{\mathrm{Cr}} = C^{\mathrm{alloy/cor,eq}}_{\mathrm{Cr}}; \quad C^{\mathrm{alloy,int1}}_{\mathrm{Al}} = C^{\mathrm{alloy/cor,eq}}_{\mathrm{Al}}; \quad C^{\mathrm{alloy,int1}}_{\mathrm{O}} = C^{\mathrm{alloy/cor,eq}}_{\mathrm{O}}; \\ &C^{\mathrm{cor,int1}}_{\mathrm{Cr}} = C^{\mathrm{cor/alloy,eq}}_{\mathrm{Cr}}; \quad C^{\mathrm{cor,int1}}_{\mathrm{Al}} = C^{\mathrm{cor/alloy,eq}}_{\mathrm{Al}}; \quad C^{\mathrm{cor,int1}}_{\mathrm{O}} = C^{\mathrm{cor/alloy,eq}}_{\mathrm{O}}; \\ &C^{\mathrm{cor,int2}}_{\mathrm{Cr}} = C^{\mathrm{cor/spinel,eq}}_{\mathrm{Cr}}; \quad C^{\mathrm{cor,int2}}_{\mathrm{Al}} = C^{\mathrm{cor/spinel,eq}}_{\mathrm{Al}}; \quad C^{\mathrm{cor,int2}}_{\mathrm{O}} = C^{\mathrm{cor/spinel,eq}}_{\mathrm{O}} \end{aligned} \tag{13}$$

The equilibrium concentrations of Cr, Al and O at the alloy/corundum and corundum/spinel interfaces are deduced from free energy minimization techniques using THERMOCALC™ and its associated databases (TTNI7). The details of the thermodynamic calculation are given in an earlier study [2]. In principle, Eqs. (6)–(11) can be solved simultaneously under the initial and boundary conditions given by Eqs. (12) and (13) to determine the elemental concentration profiles of Cr, Al and O in the alloy, corundum and spinel phases as a function of time as well as the rate of growth of the oxide phase. The diffusion equations were solved using a finite difference method (FDM). A second order spatial discretization and an explicit temporal discretization scheme were used to implement the FDM based approach. Utilizing the initial and boundary conditions and explicit time stepping, the elemental concentration profile for the next time step was computed. Based on the elemental concentration profile and thermodynamic estimate of equilibrium concentration at the interface, the boundary position was updated and based on the new boundary position, the diffusivities were updated. Although the computational algorithm can be scaled to handle multiple oxide phases this was not done in the present study because of the absence of experimental diffusivity data for the various elements and parabolic rate constants for the growth of spinel and monoxide (NiO) phases in multi-component Ni-base alloys.

2.4. Cyclic oxidation model

Since both gas turbines and aero-engines undergo periodic start-ups involving heating cycles and shutdowns involving cooling cycles, Ni-base superalloys used in these applications undergo cyclic oxidation. In cyclic oxidation, some spalling of the scale occurs during the cooling cycle. Several cyclic oxidation spalling models have been reported in the literature [1,10–13]. Typically,

in all these models, a scale growth law with a fixed rate constant is postulated for each heating cycle and a spalling formalism is defined, which governs the type and amount of spalling that occurs in each cooling cycle. Two types of cyclic spalling formalisms have been reported in the literature. In the first method, a discrete and constant area fraction of each portion of the scale spalls in each cycle [10]. In the second method, a uniform external layer of specified thickness spalls off the entire area [11–13]. The entire cyclic oxidation curve is then generated from the resultant effect of all the cycles either by series summation or by using iterative procedures. A consolidated cyclic oxidation spalling computer program (COSP), which allows the selection of various scale growth laws, spalling functions, and spalling configurations is available [12,13]. More recently, Smialek [1] has modified the interfacial spallation model (deterministic interfacial cyclic oxidation spallation model) stipulating that the spallation occurs from a constant area fraction biased towards the thickest oxide regions that is yet to spall, but does not stipulate that a critical oxide thickness be attained before spallation. Smialek [1] has also simplified the mathematics of the treatment to describe the total cyclic oxidation curve through simple algebraic functions. In his model (DICOSM), the expression for weight change (ΔW) per unit area (A) as a function of time for cyclic oxidation is given as:

$$\left(\frac{\Delta W}{A}\right)_{\text{Case A}} = F_A\sqrt{k_p\Delta t}\left\{\frac{1}{2}(2n_0 - S_c)(j)^{1/2} + \frac{1}{3}(1-2S_c)(j)^{1/2}\right\}$$

$$\left(\frac{\Delta W}{A}\right)_{\text{Case B}} = F_A\sqrt{k_p\Delta t}\left\{\left((1-S_c)j - \frac{1}{2}S_c\right)(n_0)^{1/2} + \frac{1}{3}(1+S_c)(n_0)^{3/2}\right\} \quad (14)$$

where k_p is the parabolic growth rate constant for isothermal oxidation, F_A is the spall area fraction (also known as spall constant), S_c is the weight of the oxide relative to oxygen and is constant for a given oxide and Δt is the cycle duration. Case A corresponds to the situation where the number of cycles $j \leqslant N_0$, where $N_0 = 1/F_A$, and Case B corresponds to a situation when number of cycles $j > N_0$. It is to be noted that the spall constant will be different for different alloys. We have provided a method to simulate the cyclic oxidation process. However, it is imperative for a user to utilize the experimental spall constant for a specific alloy to predict the cyclic oxidation rate. The simplified DICOSM model of Smialek [1] has been used in the present study for the prediction of cyclic oxidation of multi-component Ni-base alloys using the isothermal oxidation rates determined from the modified Wagner's equation and the coupled diffusion equations.

2.5. Evaluation of diffusivities of Cr, Al and O in the corundum phase

The mobility of most elements in Ni-base superalloys and their temperature dependence are available and included in the DICTRA™ [9] database. The chemical diffusion coefficients in any phase are determined from the mobility and activity coefficients of the respective element in the relevant phase, which is derived from THERMOCALC™ [9]. In this study, we have considered the oxide phase to be a solid solution of Al_2O_3 and Cr_2O_3. Hence, diffusivities of elements in both Chromia and Alumina have been considered.

The diffusivities of elements in oxides are not by atomic mobility but by ionic mobility and occur through the presence of charged defects (typically, cation interstitials, cation vacancies, anion vacancies, electrons, and holes). The nature, concentration, and mobility of these charged defects are a function of chemical composition, oxygen partial pressure, and temperature. Therefore, knowledge of the defect chemistry as a function of oxygen partial pressure and temperature of the various oxide phases is essential to estimate the diffusivities of the charged defects and correlation to the parabolic rate constant. The defect structure of pure Cr_2O_3 has been reviewed by Kroger [14]. It is suggested that pure Cr_2O_3 is a p-type conductor at high p_{O_2} and low temperatures and is "intrinsic" at temperatures above 1200 °C. Several researchers have reported diffusivities of Cr^{3+} cations and oxygen anions in pure Cr_2O_3. However, the results vary by 4–7 orders of magnitude. The above-mentioned results are summarized in the review papers by Hindam and Whittle [15] and Atkinson [16]. The large difference in the reported diffusivities is attributed to the domination of dislocation and grain boundary effects in many of the earlier measurements.

The variation of self-diffusivity of Cr (D^*_{Cr}) with oxygen partial pressure shows a $p_{O_2}^{-3/16}$ dependence at low p_{O_2} as would be expected from a Cr^{3+} interstitials diffusion mechanism. We initially adopted the Cr interstitials diffusivity reported by Hagel and Seybolt [17] for the corundum phase. Oxygen anion diffusion in pure Cr_2O_3 has been reported by Hagel [18] and Oishi and Kingery [19] to be three orders of magnitude slower than Cr interstitials. Oxygen anion diffusion in Cr_2O_3 reported by Hagel was initially used in the present calculations for the corundum phase. Cation and anionic diffusivities in Cr_2O_3 scale formed on alloys may be different because of the formation of oxide solid solution. Tsai and coworkers [20] report the bulk and grain boundary diffusivities of Cr interstitials and oxygen ions in Cr_2O_3 scale formed on Ni-Cr alloys and conclude that the scale growth is controlled by countercurrent diffusion of both Cr^{3+} and O^{2-} ions and that the diffusion is predominantly along grain boundaries. Lobnig et al. [21] have also measured and reported lattice and grain boundary diffusivities at 1173 K of some cations (Fe, Mn, Cr and Ni) in Cr_2O_3 scales of Fe–Cr and Fe–Cr–Ni alloys. Although they did not observe any significant difference in the lattice diffusivities of these cations, they observed that the grain boundary diffusion of Mn is the fastest and Ni is the slowest.

In the case of oxidation of corundum Al_2O_3, since Al melts at a relatively low temperature, the oxidation studies reported in the literature are essentially on alloys. Pure α-Al_2O_3 has a low concentration of ionic and electronic defects and the defect chemistry of pure α-Al_2O_3 as a function of oxygen partial pressure and temperature is still not well understood [14]. It is reported that for α-Al_2O_3, the concentration of intrinsic point defects is very small and that transport properties are dominated by solute ions present as impurities. The diffusivities of O^{2-} in α-Al_2O_3 measured and reported by several researchers and that of Al^{3+} in α-Al_2O_3 measured by Paladino and Kingery [22] have been critically reviewed and compiled by Atkinson [16]. The reported anion diffusivities vary by 3–4 orders of magnitude. Atkinson concluded that $D^*(Al)$ is always greater than $D^*(O)$ in the Al_2O_3 lattice. Despite the higher diffusivities of Al, they inferred from studies on scale morphology and marker diffusion experiments that Al_2O_3 grows by inward diffusion of oxygen. They suggest that the diffusion paths of oxygen in Al_2O_3 are the grain boundaries and fissures. However, more recently, Tolpygo and Clark [23] have produced microstructural evidence to indicate that Al_2O_3 scales grow by counter-diffusion of aluminum and oxygen in Fe–Cr–Al alloys and nickel aluminides. It is therefore clear that the diffusivities, concentration, and mobility of the mobile species in pure Cr_2O_3 and Al_2O_3 oxide are a complex function of alloy composition, oxygen partial pressure, and temperature. No experimental measurements are reported in the literature on the corundum solid solution phase involving more than one oxide.

There is much less information on the defect structure and diffusivities of Cr, Al, Ni and O in the spinel phase. Armijo [24] and Schmalzried [25] have reviewed diffusion in the spinel phase. Since

Table 1
Alloy compositions and corresponding experimental parabolic rate constants for datasets used in the optimization process.

Alloy composition atom percent	Temperature of oxidation (°C)	Parabolic rate constant ($mg^2\ cm^{-4}\ s^{-1}$)
Ni–24.7Cr–14.6Al [29]	1100	0.7×10^{-6}
Ni–25.34Cr–14.1Al–0.59Y [29]	1100	1.6×10^{-6}
Ni–10.0Cr–10.95Al–7.8Ti [30]	1000	5.0×10^{-7}
Pure Ni_3Al [31]	1100	$\log k_P = 1.8996 - 9978.3/T$
Pure Ni_3Al [15]	1100	8.987×10^{-6}
Ni–16Cr–6Al–0.1Y [15]	1100	4.25×10^{-7}
Ni–5Cr–1Al [27]	1100	$\log k_P = 7.1682 - 13{,}474/T$
Ni–30Cr–2Al [27]		$\log k_P = 5.4043 - 13{,}314/T$
Ni–5Cr–6Al [27]		1.373×10^{-6} at 1100 °C
Ni–27Cr–9Al [8]		4.862×10^{-6}
Ni–27Cr–9Al [8]	1100	5.835×10^{-6}
Ni–31Cr–20.7Al [32]	1100	0.7×10^{-6}
Ni–36.4Cr–14.1Al [32]	1100	0.6×10^{-6}
Ni–24.8Cr–24.6Al [32]	1100	1.0×10^{-6}
Ni–37.6Cr–19.0Al [32]	1100	0.8×10^{-6}
Ni–24.2Cr–21.7Al [32]	1100	0.9×10^{-6}
Ni–35.6Cr–18.0Al [32]	1100	0.3×10^{-6}
Ni–24.3Cr–22.3Al [32]	1100	0.5×10^{-6}
Ni–31.3Cr–14.7Al [32]	1100	1.0×10^{-6}
Ni–29.5Cr–24.0Al [32]	1100	1.4×10^{-6}
Ni–32.4Cr–15.35Al–0.44Y [33]	1100	7.583×10^{-7} at 900 °C and 1.228×10^{-6} at 1000 °C
Ni–19.8Cr–19.05Al–0.29Y [34]	900 and 1000	1.04×10^{-6}
Ni–15Cr–5Al–5Pd [35]	1000	3.0×10^{-6}
Ni–7.10Al–10.0Cr [33]	1100	1.18×10^{-6}
Ni–27.33Cr [36]	1100	1.478×10^{-6}
Ni–28.62Cr–0.07Y [36]	1050	7.09×10^{-7}
Ni–25.21Cr–0.47Mn [36]	1050	7.21×10^{-6}
Ni–26.92Cr–0.096Y–0.51Mn [36]	1050	5.07×10^{-6}
β–NiAl + 0.1 at.% Hf [37]	1050	$0.76–1.0 \times 10^{-6}$
Ni–22Cr–3Si [38]	1200	7.2×10^{-8}
Ni–32.6Cr [39]	900	1.4×10^{-7}
Ni–32.6Cr [39]	900	2.4×10^{-7}
Ni–32.6Cr [39]	900	6.4×10^{-7}
Ni–30.5Cr [40]	900	9×10^{-6}
Ni–30.18Cr–22.08Fe [40]	1000	1.1×10^{-5}
Ni–30.54Cr–26.94Co [41]	1000	1.9×10^{-5}
Ni–29.66Cr–5.30Si [41]	1000	2.9×10^{-6}
Ni–29.35Cr–21.47Fe–5.24Si [41]	1000	2.6×10^{-6}
Ni–29.7Cr–26.2Co–5.30Si [41]	1000	3.2×10^{-6}
Ni–27.33Cr–0.1Ti [42]	1000	5.338×10^{-6}
Ni–27.33Cr–0.1Cr [42]	1000	4.185×10^{-6}
Ni–27.33Cr–0.1Mn [42]	1000	7.809×10^{-6}
Ni–27.33Cr–0.1Sc [42]	1000	8.328×10^{-6}
Ni–27.33Cr–0.1Nb [42]	1000	5.990×10^{-6}
Ni–27.33Cr–0.1 Mg [42]	1000	4.684×10^{-6}
Ni–27.33Cr–0.1Hf [42]	1000	2.979×10^{-6}
Ni–27.33Cr–0.1Zr [42]	1000	1.634×10^{-6}
Ni–27.33Cr–0.1Ca [42]	1000	8.918×10^{-6}
Ni–27.33Cr–0.1Y [42]	1000	6.167×10^{-7}
Ni–27.33Cr–0.1Ce [42]	1000	1.471×10^{-7}
Ni–27.33Cr–0.1 Tb [42]	1000	3.310×10^{-7}
Ni–27.33Cr–0.1Gd [42]	1000	1.764×10^{-7}
Ni–27.33Cr–0.1Sm [42]	1000	1.921×10^{-7}
Ni–27.33Cr–0.1Nd [42]	1000	1.921×10^{-7}
Ni–27.33Cr–0.1La [42]	1000	2.002×10^{-7}

sufficient experimental information on the growth rates of Ni-base spinel oxide layers is not available, the growth of the spinel phase could not be considered in the present study and the growth of only the corundum phase is considered. However, the formation of spinel phase in equilibrium with corundum as thermodynamically predicted is acknowledged.

The defect chemistry and consequently the transport mechanism and their oxygen partial pressure dependence in oxide solutions (corundum, spinel etc.) will differ considerably. Since no measurements exist in the literature on the diffusivities in oxide solid solutions, an attempt was made to estimate the effective diffusivities of Cr, Al and O in the corundum solid solution and their temperature and oxygen partial pressure dependence from the experimental parabolic rate constants for several ternary Ni–Cr–Al and quaternary Ni–Cr–Al–X alloys by applying the Wagner's equation (Eq. (4)) through an optimization procedure. A genetic algorithm (GA) based optimization scheme has been used to estimate the effective diffusivities (D^*_{eff}) and the pressure dependence parameters (n_i) of the three diffusing species (Cr, Al and O). The algorithm implemented in the present study is a modified version of a differential evolution type GA [26] that can handle both constrained and unconstrained optimization problems. No initial guesses are required for this optimization method. Thirty-seven experimental data sets of parabolic rate constants for Ni-base ternary and quaternary alloys at 1373 K were used to extract the optimum value of the six unknown parameters ($D^{\text{eff}}_{\text{Cr}}$, $D^{\text{eff}}_{\text{Al}}$, D^{eff}_{O} at 1373 K and their individual p_{O_2} dependences). The Arrhenius energies for these diffusivities were then deduced from the experimental temperature dependent parabolic rate constants for some of these alloys available in the literature. These parameters were then used to compute the oxidation rate of the multi-component Ni-base superalloys (*viz.* Ni–5Cr–6Al, Ni–20Cr–6Al, CMSX-4, and Rene'

N5). The equilibrium oxygen partial pressures at the alloy/corundum and corundum/spinel interface for all these alloys required for application of Wagner's equation (Eq. (4)) to the optimization process were obtained from thermodynamic modeling through the procedure described earlier [2]. It needs to be emphasized that in the estimation of optimized diffusivities of Cr, Al and O in the corundum solid solution at 1373 K and their p_{O_2} dependence, no experimental information on multi-component Ni-base alloys were used. The estimated diffusivities as a function of temperature and oxygen partial pressure were then used to calculate the oxide growth rates in multi-component Ni-base superalloys using the Wagner's model (Eq. (4)). Solving the diffusion equations also yields the elemental concentration profile in the corundum solution as a function of time of oxidation.

Table 2
Optimized self-diffusivities of Cr, Al and O in the corundum phase and their oxygen partial pressure dependencies.

Element	D (cm^2/s)	n
Cr	6.86224×10^{-19}	−4.99438
Al	8.60143×10^{-21}	−4.838524
O	2.60328×10^{-19}	−4.998994

3. Results and discussion

The datasets of alloy compositions, the corresponding experimental parabolic rate constants, and the equilibrium oxygen partial pressures at the alloy-corundum and corundum-spinel interface determined from THERMOCALC™ used for the optimization process are summarized in Table 1. The optimized self-diffusivities of Cr, Al and O in corundum phase, their oxygen partial pressure, and temperature dependences are summarized in Table 2. The results indicate that the diffusivities of Cr interstitials and oxygen ions at 1373 K are of the same order of magnitude and that of aluminum interstitials are two orders of magnitude smaller. However, the diffusivity of Cr interstitials is the fastest among the three species. It is also interesting to note that the optimized p_{O_2} dependence of the diffusivities of all the three species is very similar (−1/5) to what would be expected if Cr^{3+} interstitials were the main diffusing species (self-diffusivity of Cr with oxygen partial pressure shows a $p_{O_2}^{-3/16}$ dependence in pure Cr_2O_3 [17].

The agreement between the experimental parabolic rate constants at 1373 K and those calculated from the optimized diffusivities are shown in Fig. 1. It is seen that the agreement between the two is very good. The rates of the corundum phase formation were determined for four multi-component Ni-base alloys (Ni–5Cr–6Al, Ni–26Cr–4.5Al, CMSX-4 and Rene' N5) using the optimized diffusivities. The equilibrium oxygen partial pressures, the elemental

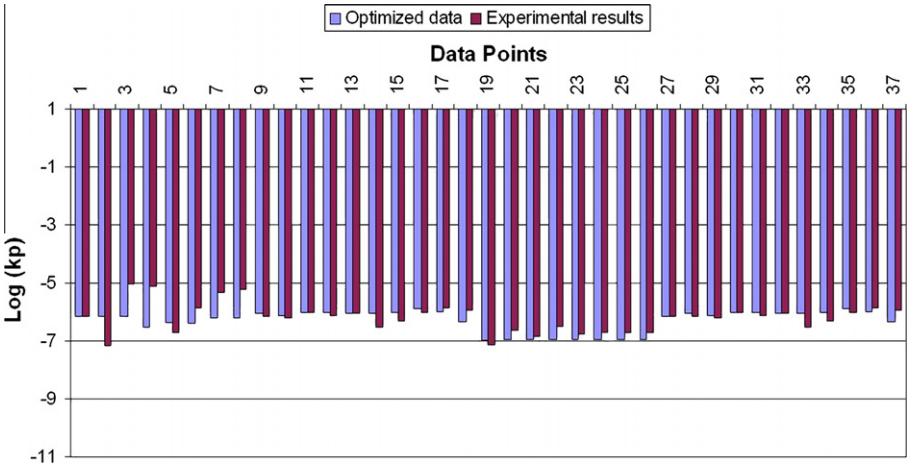

Fig. 1. Comparison of the experimental and optimized parabolic rate constants for several ternary Ni–Cr–Al and quaternary Ni–Cr–Al–X alloys at 1373 K (for the alloy classifications see Table 1).

Table 3
Thermodynamic modeling of equilibrium p_{O_2} and elemental concentrations at interfaces of oxidized Ni-base alloys.

Temp. (K)	Alloy–corundum interface					Alloy–corundum–spinel interface					Spinel–bunsenite_NiO interface				
	ln p_{O_2} (atm)	X_{Ni}	X_{Cr}	X_{Al}	X_O	ln p_{O_2} (atm)	X_{Ni}	X_{Cr}	X_{Al}	X_O	ln p_{O_2} (atm)	X_{Ni}	X_{Cr}	X_{Al}	X_O
Ni–27Cr–9Al (at.%) i.e., Ni–25.98Cr–4.49Al (wt.%) alloy															
1373	−43.23	0.64	0.27	0.09	1.1e-6	−27.30	0.10	0.27	0.09	0.54					
Ni–5Cr–6Al (wt.%) alloy															
1373	−42.30	0.826	0.052	0.121	8.8e-7	−27.29	0.635	0.044	0.102	0.219	−24.08	0.583	0.042	0.097	0.279
1473	−39.62	0.826	0.052	0.121	9.3e-7	−25.86	0.635	0.044	0.102	0.219	−22.82	0.583	0.042	0.097	0.278
Ni–20Cr–6Al (wt.%) alloy															
1473	−40.58	0.675	0.206	0.119	9.5e-7	−25.91	0.400	0.152	0.088	0.360	−22.85	0.337	0.140	0.081	0.443
CMSX-4 alloy (Ni–9Co–6.5Cr–0.6Mo–6.0W–5.6Al–1.0Ti–6.5Ta–0.1Hf–3Re)															
1373	−43.16	0.638	0.076	0.126	1.0e-6	−26.81	0.446	0.061	0.102	0.261	−23.64	0.400	0.058	0.096	0.323
1450	−41.16	0.638	0.076	0.126	1.14e-6	−25.70	0.446	0.061	0.102	0.261	−22.67	0.400	0.058	0.096	0.323
Rene' N5 alloy (Ni–7.5Co–7Cr–1.5Mo–5W–6.2Al–7Ta–0.15Hf–3Re)															
1366	−43.28	0.644	0.081	0.139	9.6e-7	−27.00	0.447	0.065	0.112	0.266	−23.65	0.397	0.061	0.105	0.333

chemical potentials, and concentrations at the alloy-corundum and corundum-spinel interface computed by thermodynamic modeling for all these alloys are listed in Table 3. For simplicity, only the corundum phase was assumed to form and the formation of other oxide phases (spinel and monoxide) were neglected.

The rates of oxidation of ternary Ni–5Cr–6Al wt.% and Ni–20Cr–6Al alloy at 1373 K computed from Wagner's equation are shown in Fig. 2a and b and are compared with the experimental results of Giggins and Pettit [27] for these alloys. It is seen that for both these alloys, the agreement between the predicted and experimental isothermal oxidation rates is excellent. The experimental results were not used for the optimization process.

The isothermal oxidation rates of a commercial alloy CMSX-4 at 1373 K determined using the present approaches is compared with the experimental results of Mu et al. [28] in Fig. 2c. Similarly the oxidation rate of Rene' N5 determined from Wagner's model is shown in Fig. 2d and compared with the experimental results [45]. The predicted results for Rene' N5 are in very good agreement with the experimental data. However, for CMSX-4, the model under-predicts the oxidation rate.

The isothermal oxidation rate of Rene' N5 alloy at 1373 K, determined independently by solution of the elemental diffusion and mass balance equations using the initial and boundary conditions, is shown in Fig. 3. Although we do not have any direct evidence about the mechanism of defect migration, our optimization procedure yielded a p_{O_2} dependence of $n = 3/16$ for all the three diffusivities. This value is very close to that expected for Cr interstitial diffusion ($n = 1/5$) in pure Cr_2O_3 [17]. In this case, the oxidation rate is determined purely by the fastest diffusing species i.e., Cr (see Table 2) and therefore among the mass balance equations formulated, only the one corresponding to Cr is applied. Further we have assumed the atomic diffusion coefficient and the ionic diffusion coefficient in corundum to be identical for solving the diffusion equations. The oxidation rate or the rate of corundum phase formation calculated using this approach overestimates the oxidation rate considerably. For example in 250 h, the oxide scale thickness predicted by Wagner theory is ~2 μm in comparison to 7 μm predicted by the diffusion model. The prediction of oxidation rates using the diffusion model can be improved by altering the atomic diffusivities of Cr, Al and O. This has not been carried out in the present study because atomic diffusion is inconsistent with the generally accepted mechanism of defect diffusion in oxide scales.

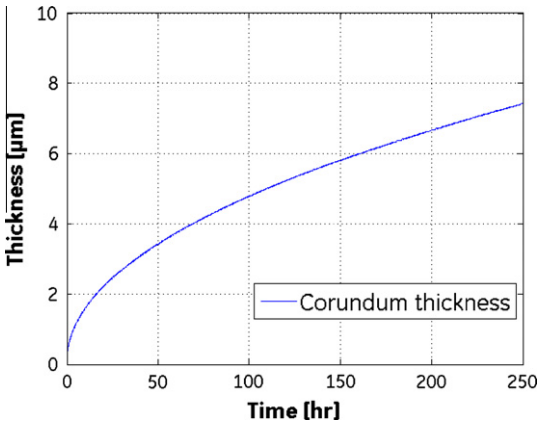

Fig. 3. Oxidation thickness vs. time, as predicted by the kinetic diffusion model.

The cyclic oxidation rates for these alloys (Rene' N5 and CMSX-4) determined from the DICOSM model (Eq. (14)) using the isothermal parabolic rate constants determined through Wagner's

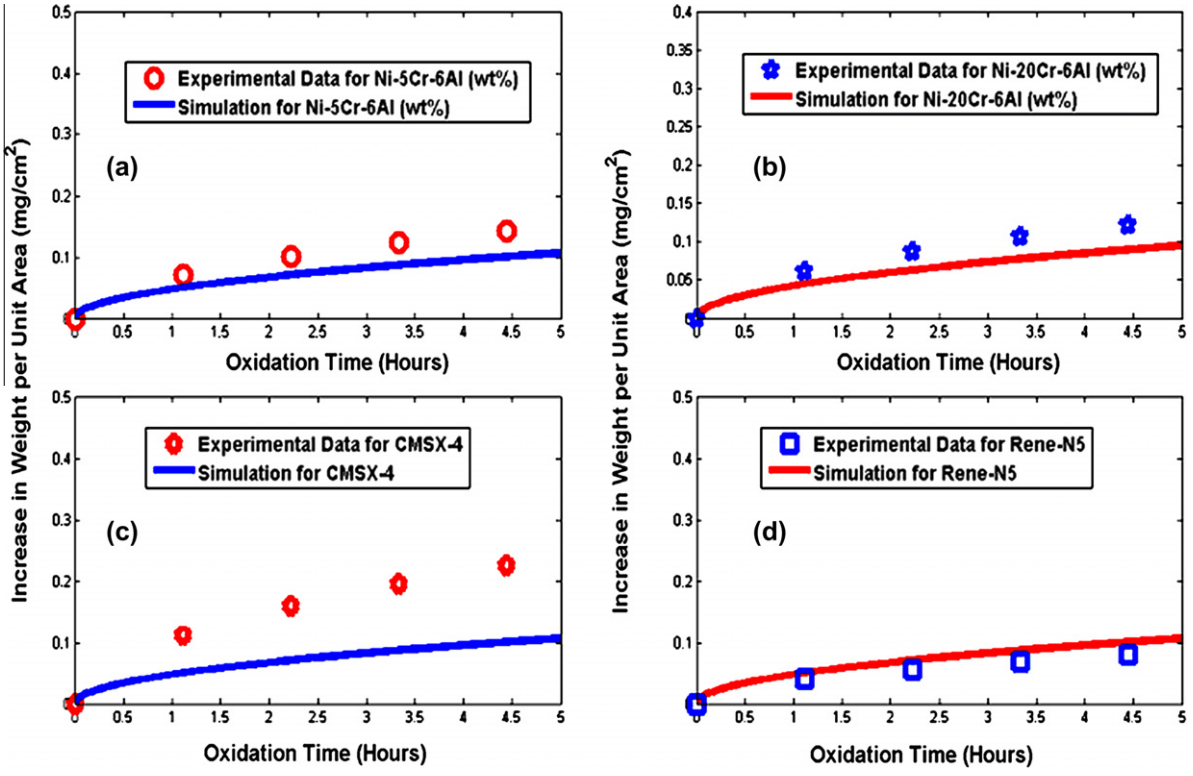

Fig. 2. (a) Comparison of the predicted and experimental rates of oxidation of Ni–5Cr–6Al alloy at 1373 K. (b). Predicted vs. experimental isothermal oxidation rates of Ni–20Cr–6Al (wt.%) alloys at 1373 K. (c). Isothermal oxidation of Ni-base superalloy CMSX-4 – comparison of prediction with experimental results at 1373 K. (d) Comparison of the predicted and experimental rates of isothermal oxidation of Rene' N5 at 1373 K.

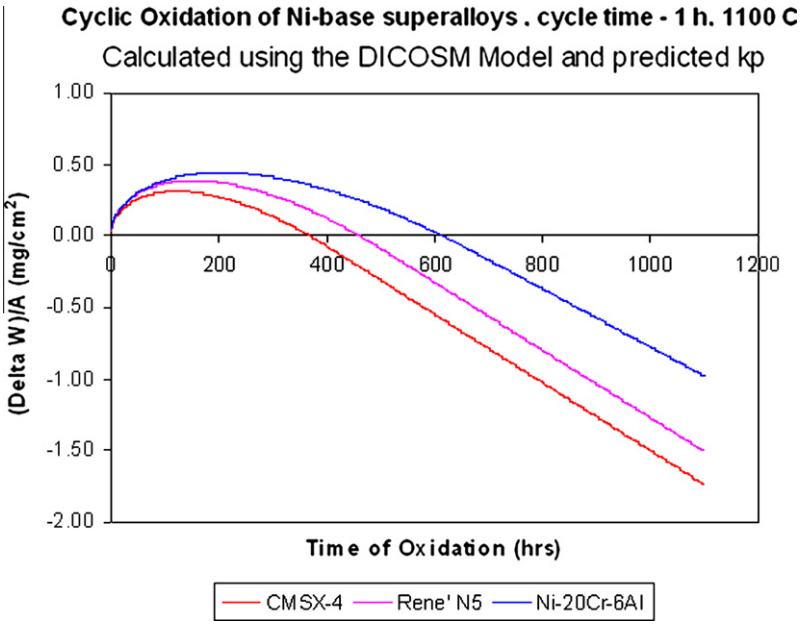

Fig. 4. Computed (from DICOSM model) cyclic oxidation rate of Ni–5Cr–6Al, CMSX-4 and Rene' N5 at 1173 K. The spall area fraction (F_A) for these computations was 0.0025.

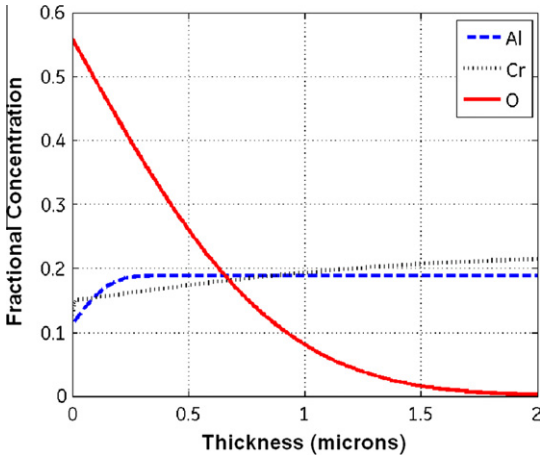

Fig. 5. Calculated concentration profiles of Cr, Al and O in the corundum phase at 1373 K for Rene' N5 after 250 h of oxidation.

equation and solution of diffusion equation are delineated in Fig. 4. For some of the Ni–Cr–Al–Y alloys for which cyclic oxidation data were available, it was found that the model predictions are close to the experimental values at $F_A = 0.0025$. Experimental cyclic oxidation rates for these alloys were not available to make a comparison.

The elemental concentration profiles of Cr, Al and O were calculated at 1373 K for Rene' N5 using the diffusion equations and the initial and boundary conditions. These are shown in Fig. 5. Experimental information on the concentration profile in the oxide scale for these alloys is not available in the literature for comparison. Please note that the concentrations have been normalized. Also, the oxide phase is considered as solution and only the mobile species participate in the diffusion, and subsequent oxidation, process. Thus the variation of oxygen species from 0.55 (at the oxide–air interface) to 0 (at the oxide–alloy interface) is represented by the mobile oxygen atoms, which participate in the alloy oxidation process. Fig. 5 gives a snapshot of the concentration profile of the mobile species after 250 h of oxidation. A steady-state concentration profile will have a discreet change at the oxide-air interface and alloy–oxide interface.

4. Conclusions

Two new approaches have been presented for the prediction of the oxidation rates of multi-component Ni-base alloys by combining thermodynamic and kinetic modeling. One based on the solution of the elemental diffusion equations under mass balance constraints and thermodynamically computed boundary conditions, and the other based on a modified Wagner's equation with the limiting equilibrium oxygen partial pressured derived by thermodynamic modeling. In this study, we have considered the oxide phase to be a solid solution of Al_2O_3 and Cr_2O_3. Hence, diffusivities of elements in both Chromia and Alumina have been considered. Optimized values of diffusivities of Cr, Al and O in the mixed oxide phase (Al_2O_3 and Cr_2O_3) and their oxygen partial pressure and temperature dependences have been derived. Next, those are used for the prediction of oxidation rates and elemental concentration profile in the oxide phase. The oxygen partial pressure dependence was found to correspond to Cr^{3+} interstitials diffusion in the oxide phase. Even though both these approaches can predict the oxidation rates, the solution of the elemental diffusion equations was found to over-predict the oxidation rates. The modified Wagner's equation was found to predict the oxidation rate of the multi-component alloys tested in this study well.

Acknowledgement

The authors will like to acknowledge Kelly Fletcher, GE Global Research, for funding this work. Useful discussions with Michael Gigliotti, GE Global Research, as well as with Andrew Elliott and Stephen Balsone of GE Energy are also acknowledged.

References

[1] J.L. Smialek, Acta Mater. 51 (2003) 469–483.
[2] P. Saltykov, O. Fabrichnaya, J. Golczewski, F. Aldinger, J. Alloys Comp. 381 (2004) 99–113.
[3] C. Wagner, J. Electrochem. Soc. 99 (1952) 369–380.
[4] V.J.D. Tretjakow, H. Schmalzried, Ber. Bunsengesellschafr Phys. Chem. 69 (1965) 396–402.
[5] F. Gesmundo, Mater. Sci. Eng. 87 (1987) 243–250.
[6] R. Dieckmann, J. Phys. Chem. Solids 59 (1998) 507–525.
[7] T.J. Nijdam, L.P.H. Jeurgens, W.G. Sloof, Acta Mater. 51 (2003) 5295–5307.

[8] T.J. Nijdam, L.P.H. Jeurgens, W.G. Sloof, Acta Mater. 53 (2005) 1643–1653.
[9] THERMOCALC™ Software URL. <http://www.thermocalc.com/>.
[10] J.L. Smialek, Metall. Trans. 9A (1978) 309–320.
[11] C.E. Lowell, J.L. Smialek, C,A. Barrett, Cyclic oxidation of superalloys, in: R.A. Rapp (Ed.), High Temperature Corrosion, Houston, TX-NACE, 1983, pp. 219–226.
[12] C.E. Lowell, C.A. Barrett, R.W. Palmer, J.V. Auping, H.B. Probst, Oxid. Met. 36 (1991) 81–112.
[13] J.L. Smialek, J.V. Auping, Oxid. Met. 57 (2002) 559–581.
[14] F.A. Kroger, Defects and transport in SiO_2, Al_2O_3 and Cr_2O_3, in: R.A. Rapp (Ed.), High Temperature Corrosion, NACE 6, National Association of Corrosion Engineers, Houston, 1983, pp. 89–94.
[15] H. Hindam, D.P. Whittle, Microstructure, adhesion and growth kinetics of protective scales on metals and alloys, Oxid. Met. 18 (1982) 245–284.
[16] A. Atkinson, Rev. Mod. Phys. 57 (1985) 437–470.
[17] W.C. Hagel, A.U. Seybolt, J. Electrochem. Soc. 108 (1961) 1146–1152.
[18] W.C. Hagel, J. Am. Ceram. Soc. 48 (1965) 70–75.
[19] Y. Oishi, W.D. Kingery, J. Chem. Phys. 33 (1960) 480–486.
[20] S.C. Tsai, A.M. Huntz, C. Dolin, Mater. Sci. Eng. A212 (1996) 6–13.
[21] R.E. Lobnig, H.P. Schmidt, K. Hennesen, H.J. Grabke, Oxid. Met. 37 (1992) 81–93.
[22] A.E. Paladino, W.D. Kingery, J. Chem. Phys. 37 (5) (1962) 957–962.
[23] V.K. Tolpygo, D.R. Clarke, Microstructural evidence for counter-diffusion of aluminum and oxygen during the growth of alumina scales, in: 5th International Conference on the Microscopy of Oxidation, University of Limerick, Republic of Ireland, 2002 (26–28 August).
[24] J.S. Armijo, Oxid. Met. 1 (1969) 171–198.
[25] H. Schmalzried, Prog. Chem. Solid State 2 (1965) 265–303.
[26] V.K. Price, M.R. Storn, A.J. Lampinen, Differential Evolution: A Practical Approach to Global Optimization, Springer, Berlin, 2005.
[27] C.S. Giggins, F.S. Pettit, J. Electrochem. Soc. 118 (11) (1971) 1782–1790.
[28] N. Mu, J. Liu, J.W. Bycon, Y.H. Sohn, Y.L. Nava, Surf. Coat. Technol. 188–189 (2004) 27–34.
[29] P. Choqueta, C. Indrigoa, R. Mevrel, Mater. Sci. Eng. 88 (1987) 97–101.
[30] G.F. Chen, H.Y. Lou, Mater Lett. 45 (2000) 286–291.
[31] S.C. Choi, H.J. Cho, Y.J. Kim, D.B. Lee, Oxid. Met. 46 (1996) 51–72.
[32] S. Han, D.J. Young, Mater. Res. 7 (2004).
[33] B. Wang, J. Gong, A.Y. Wang, C. Sun, R.F. Huang, L.S. Wen, Surf. Coat. Technol. 149 (2002) 70–75.
[34] Y.J. Zhang, X.F. Sun, Y.C. Zhang, T. Jin, C.G. Deng, H.R. Guan, Z.Q. Hu, Mater. Sci. Eng. A 360 (2003) 65–69.
[35] N.S. Miller, G. Simkovich, E.J. Whitney, J. Mater. Sci. Lett. 19 (2000) 1657–1659.
[36] J. Zurek, D.J. Young, E. Essuman, M. Hänsel, H.J. Penkalla, L. Niewolak, W.J. Quadakkers, Mater. Sci. Eng. A 477 (2008) 259–270.
[37] B.A. Pint, Surf. Coat. Technol. 188–189 (2004) 71–78.
[38] J.M. Brossard, J. Balmain, F. Sanchette, G. Bonnet, Oxid. Met. 64 (2005) 43–61.
[39] H.L. Tsai, P.C. Tsai, Surf. Coat. Technol. 71 (1995) 53–59.
[40] M.H. Li, X.F. Sun, J.G. Li, Z.Y. Zhang, T. Jin, H.R. Guan, Z.Q. Hu, Oxid. Met. 59 (2003) 591–605.
[41] M.H. Li, X.F. Sun, T. Jin, H.R. Guan, Z.Q. Hu, Oxid. Met. 60 (2003) 195–210.
[42] B.A. Pint, P.F. Tortorelli, I.G. Wright, Oxid. Met. 58 (2002) 73–101.
[43] X. Zhang, C. Gao, L. Wang, Y. Niu, Trans. Nonferrous Met. Soc. China 17 (2007) 171–174.
[44] <http://www.calphad.com/dictra.html>.
[45] <http://www.surmet.com/docs/Test_Data_ALON%20Coating.pdf>.